

Cluster Formation and The Virial Equation of State of Low-Density Nuclear Matter

C.J. Horowitz* and A. Schwenk†

Nuclear Theory Center and Department of Physics, Indiana University, Bloomington, IN 47408

We present the virial equation of state of low-density nuclear matter composed of neutrons, protons and alpha particles. The virial equation of state is model-independent, and therefore sets a benchmark for all nuclear equations of state at low densities. We calculate the second virial coefficients for nucleon-nucleon, nucleon-alpha and alpha-alpha interactions directly from the relevant binding energies and scattering phase shifts. The virial approach systematically takes into account contributions from bound nuclei and the resonant continuum, and consequently provides a framework to include strong-interaction corrections to nuclear statistical equilibrium models. The virial coefficients are used to make model-independent predictions for a variety of properties of nuclear matter over a range of densities, temperatures and compositions. Our results provide constraints on the physics of the neutrinosphere in supernovae. The resulting alpha particle concentration differs from all equations of state currently used in supernova simulations. Finally, the virial equation of state greatly improves our conceptual understanding of low-density nuclear matter.

PACS numbers: 21.65.+f, 26.50.+x, 97.60.Bw, 05.70.Ce

Keywords: Low-density nuclear matter, equation of state, clustering, virial expansion

I. INTRODUCTION

What do we mean by nuclear matter at subsaturation density? This is an important conceptual question. The binding energy of uniform nuclear matter has a minimum at saturation density $n_0 \approx 0.16 \text{ fm}^{-3}$. Below this density, the system can minimize its energy by forming clusters. Therefore the study of low-density nuclear matter is a study of clusters. What are the properties of these clusters? What role do they play in astrophysics? What is the relationship between clusters formed in the thermodynamic limit for an infinite system and those formed in laboratory heavy-ion collisions? In this paper, we answer these questions using the virial expansion for low-density nuclear matter.

Simulations of core-collapse supernovae [1, 2], giant stellar explosions, depend on properties of low-density nuclear matter near the neutrinosphere. If one views a star in visible light, one sees the photosphere. This is the surface of last scattering for photons. Supernovae emit 99% of their energy in neutrinos, and if one views a supernova in neutrinos, one sees the neutrinosphere. This is the surface of last scattering for neutrinos and occurs at a density where the neutrino mean-free path is comparable to the size of the system. Direct evidence for the temperature of the neutrinosphere yields roughly $T \approx 4 \text{ MeV}$, from the small number of neutrinos detected in SN1987a [3, 4]. The neutrinosphere density, $n \sim 10^{11} \text{ g/cm}^3 \sim 1/1000 n_0$, then follows from known cross sections for neutrinos with these energies. *In this paper, we use the virial expansion to make model-independent predictions for the equation of state and other properties of low-density nuclear matter near the*

neutrinosphere. We will use these results in later works to calculate neutrino interactions.

Nuclear statistical equilibrium (NSE) models are commonly used in nuclear astrophysics [5]. These models describe low-density nuclear matter as a system of non- or minimally-interacting nuclei with a distribution of neutron number N and charge Z determined from nuclear masses through statistical equilibrium. However, NSE models fail in an uncontrollable manner as the density increases and strong interactions between nuclei become important. One would like a model-independent way to include strong interactions and a well-defined criterion to determine the range of validity of NSE models. In this paper we take a step towards this goal by considering a simple NSE model with neutrons (n), protons (p) and alpha (α) particles. The virial expansion is then used to systematically incorporate strong interactions using nucleon-nucleon (NN), $N\alpha$ and $\alpha\alpha$ elastic scattering phase shifts.

Pure neutron matter at low density is a very interesting nearly-universal Fermi system. In the limit that the neutron-neutron scattering length is large compared to the interparticle spacing and the range of the interaction is small, the properties of dilute Fermi gases are expected to be universal, independent of the details of the interaction. In a separate paper [6], we have calculated the equation of state of low-density neutron matter using the virial expansion, in order to assess quantitatively how close the system is to universal behavior at finite temperature. The equation of state of resonant and dilute Fermi gases has also been studied in laboratory experiments with trapped atoms [7, 8, 9, 10], and Ho *et al.* have used the virial expansion to describe Fermi gases at high temperatures in the vicinity of Feshbach resonances [11, 12].

There are many theoretical approaches to low-density nuclear matter. Microscopic calculations start from NN and three-nucleon interactions that reproduce NN

*E-mail: horowitz@indiana.edu

†E-mail: schwenk@indiana.edu

scattering and selected few-nucleon data. In addition to the conventional variational [13, 14] and Brueckner [15, 16] calculations, renormalization-group methods coupled with effective field theory provide new insights to nuclear forces and the possibility of a perturbative and thus systematic approach to nuclear matter with theoretical error estimates [17, 18]. However, all wave functions that are typically used only include two-nucleon correlations and omit four-nucleon correlations that could be important to describe alpha particle formation at low densities. We note that the equation of state calculation of Buchler and Coon [19] is close in strategy to the virial equation of state, but it takes into account Pauli blocking on the phase shifts and thus uses a model NN interaction. Moreover, there are a variety of Skyrme-type [20, 21, 22] and relativistic mean-field [23, 24, 25] parametrizations of the nuclear energy functional, which are used to calculate ground-state energies and densities of intermediate-mass and heavy nuclei. However, it is not clear what form to take for the energy functional for a gas of nucleons at low densities, where the system forms clusters and the binding energy per nucleon is density-independent with $E/A \approx -16$ MeV.

There are also some phenomenological models that attempt to provide a reasonable behavior for the equation of state over a wide range of densities, temperatures and compositions. The Lattimer-Swesty equation of state [26] is based on an extended liquid-drop model. This equation of state is almost universally used in modern supernova simulations [1, 2]. In addition, the Shen-Toki-Oyamatsu-Sumiyoshi equation of state [27] is based on an approximate Thomas-Fermi calculation using a relativistic mean-field interaction. However, it is not clear how reliable these models are, and there does not appear to be any way to systematically improve them.

Recently, there are lattice simulations for neutron matter using effective field theory [28], where the couplings are fitted to reproduce NN scattering regularized on the same lattice. These calculations are promising, but are presently limited to low orders in the effective field theory expansion and to small lattices. It is very useful to compare these lattice results to our virial equation of state at low densities. In the virial approach it is simple to assess how errors in the NN phase shifts, because of a low-order truncation in the effective field theory, impact the equation of state. The virial equation of state thus provides a valuable check for the lattice results.

The virial expansion is a very general and old method for determining the equation of state of a dilute gas. There are two major assumptions. First, that the system is in a gas phase and has undergone no phase transition with decreasing temperature or increasing density. Second, that the fugacity $z = e^{\mu/T}$ is small, so the partition function can be expanded in powers of z . Here μ denotes the chemical potential and T is the temperature. The second virial coefficient b_2 describes the z^2 term in the fugacity expansion of the partition function, while the third virial coefficient describes the z^3 term. A gen-

eral formula relating b_2 to the two-body elastic scattering phase shifts has been known for some time [29]. Little is known about the third virial coefficient [30, 31]. The first application of the virial expansion to hot matter formed in heavy-ion experiments was by Pratt *et al.* [33]. In addition, Venugopalan and Prakash [34], for example, use the virial expansion to study matter formed in relativistic heavy-ion collisions. In general, however, the latter work is interested in much higher temperatures, where thermal mesons are important.

A great advantage of the virial expansion is that it correctly includes both bound states and scattering resonances on an equal footing. In contrast, NSE models only include bound state contributions. Since the thermodynamics of the system is continuous when a bound state moves into the resonant continuum, both weakly bound states and low-energy scattering resonances are equally important. This was explicitly demonstrated for Fermi gases in the crossover region of a Feshbach resonance by Ho and Mueller [11]. The virial expansion in this paper includes contributions from the two-nucleon (deuteron) and four-nucleon (alpha particle) bound states and the relevant low-energy scattering resonances: the dominant ones being the 1S_0 two-nucleon resonance (^2He or ^2n), the $P_{3/2}$ $N\alpha$ resonance and the $\alpha\alpha$ 0^+ resonance that is the ground state of ^8Be .

This paper is organized as follows. In Section II, we present our virial formalism. Results are presented in Section III for the virial coefficients and equilibrium properties, such as the composition, pressure, entropy, energy and symmetry energy. We conclude and give an outlook in Section IV.

II. FORMALISM

In this section, we introduce the virial expansion for a system of neutrons, protons, and alpha particles. We first discuss our choice of n , p and α particle degrees of freedom. Then we present the virial equation of state expanded to second order in the fugacities and calculate the entropy and the energy. Finally, we relate the second virial coefficients to the relevant scattering phase shifts.

A. Nuclear Statistical Equilibrium

There is a close relation between the virial expansion and NSE models. The latter include a variety of bound states, while the virial expansion includes both bound states and scattering resonances. The virial equation of state can therefore also be regarded as a systematic extension of NSE models to take into account strong interactions in the resonant continuum.

The deuteron is automatically included in the virial expansion as a bound-state contribution to the second virial coefficient $b_2 \sim e^{E_d/T}$ with experimental deuteron binding energy $E_d = 2.22$ MeV. However, the α particle

has a large binding energy, $E_\alpha = 28.3$ MeV, and this will only be included in the fourth virial coefficient describing four-nucleon interactions. In general, fourth-order contributions are expected to be small at low densities and high temperatures. However, for lower temperatures $e^{E_\alpha/T}$ is very large. This will lead to an unnaturally large fourth virial coefficient that will greatly reduce the radius of convergence of the nucleonic virial expansion.

Our solution to this problem is to rearrange the original nucleonic virial expansion and include α particles explicitly. This allows us to retain the large $e^{E_\alpha/T}$ terms at lower order in the virial expansion. This procedure can be extended to explicitly include a variety of additional heavy nuclei that may be important at even higher densities. We discuss the effects of heavier nuclei and of three-nucleon contributions in more detail below. In this first paper, for simplicity, we limit ourselves to n , p and α particle degrees of freedom. We note that three-nucleon bound state effects are expected to be small, because their binding energies are small compared to E_α , and the system will thus favor the formation of alpha particles.

Therefore, we consider a low-density gas of n , p and α particles. In chemical equilibrium, the neutron μ_n , proton μ_p and alpha μ_α chemical potentials satisfy

$$2\mu_p + 2\mu_n = \mu_\alpha, \quad (1)$$

so that the neutron $z_n = e^{\mu_n/T}$, proton $z_p = e^{\mu_p/T}$ and alpha $z_\alpha = e^{(\mu_\alpha + E_\alpha)/T}$ fugacities are related by

$$z_\alpha = z_p^2 z_n^2 e^{E_\alpha/T}. \quad (2)$$

As discussed above, we will consider z_α to be the same order as z_n or z_p and expand the partition function through second order in the fugacities z_n , z_p and z_α . This is equivalent to the virial expansion with only nucleon densities at high temperatures and reduces to the virial expansion of a pure α gas at low temperatures (assuming equal numbers of n and p , $z_n = z_p$). Moreover, it is equivalent to including only the bound-state contribution in the fourth nucleon virial coefficient.

B. Virial Equation of State

We expand the grand-canonical partition function \mathcal{Q} for a system of n , p and α particles confined to a volume V as

$$\begin{aligned} \mathcal{Q}(z_n, z_p, z_\alpha, V, T) = & 1 + z_n Q_n + z_p Q_p + z_\alpha Q_\alpha \\ & + z_n^2 Q_{nn} + z_p^2 Q_{pp} + z_\alpha^2 Q_{\alpha\alpha} \\ & + 2z_p z_n Q_{np} + 2z_n z_\alpha Q_{\alpha n} \\ & + 2z_p z_\alpha Q_{\alpha p} + \mathcal{O}(z_i^3). \end{aligned} \quad (3)$$

Here, $Q_i = Q_i(V, T)$ and Q_n , Q_p and Q_α are the partition functions for single particle n , p or α systems

$$\frac{Q_n}{V} = \frac{Q_p}{V} = \frac{2}{\lambda^3} \quad \text{and} \quad \frac{Q_\alpha}{V} = \frac{1}{\lambda_\alpha^3}, \quad (4)$$

where λ (λ_α) denotes the nucleon (α particle) thermal wavelength,

$$\lambda = (2\pi/mT)^{1/2} \quad \text{and} \quad \lambda_\alpha = (2\pi/m_\alpha T)^{1/2}. \quad (5)$$

We use $m_n = m_p$ for the nucleon mass m and $m_\alpha = 4m$ for the alpha particle mass, thus $\lambda_\alpha = \lambda/2$. Below, we will relate the two-particle partition functions $Q_{ij} = Q_{ij}(V, T)$ with $i, j = n, p, \alpha$ to the second virial coefficients.

Next, we expand $\log \mathcal{Q}$ to second order in the fugacities

$$\begin{aligned} \frac{\log \mathcal{Q}}{V} = & 2 \frac{z_n}{\lambda^3} + 2 \frac{z_p}{\lambda^3} + \frac{z_\alpha}{\lambda_\alpha^3} + z_n^2 \frac{Q_{nn} - \frac{1}{2} Q_n^2}{V} \\ & + z_p^2 \frac{Q_{pp} - \frac{1}{2} Q_p^2}{V} + z_\alpha^2 \frac{Q_{\alpha\alpha} - \frac{1}{2} Q_\alpha^2}{V} \\ & + 2z_p z_n \frac{Q_{np} - \frac{1}{2} Q_n Q_p}{V} + 2z_p z_\alpha \frac{Q_{\alpha p} - \frac{1}{2} Q_\alpha Q_p}{V} \\ & + 2z_n z_\alpha \frac{Q_{\alpha n} - \frac{1}{2} Q_\alpha Q_n}{V} + \mathcal{O}(z_i^3). \end{aligned} \quad (6)$$

We define the second neutron virial coefficient b_n as

$$b_n = \frac{\lambda^3}{2V} (Q_{nn} - \frac{1}{2} Q_n^2) \approx \frac{\lambda^3}{2V} (Q_{pp} - \frac{1}{2} Q_p^2), \quad (7)$$

where the second approximation is due to neglecting the Coulomb interaction between protons and assumes charge-independent nuclear interactions. Likewise, the second alpha virial coefficient b_α is given by

$$b_\alpha = \frac{\lambda_\alpha^3}{V} (Q_{\alpha\alpha} - \frac{1}{2} Q_\alpha^2), \quad (8)$$

and the virial coefficients describing strong interactions between pn and $N\alpha$ particles are

$$b_{pn} = \frac{\lambda^3}{2V} (Q_{np} - \frac{1}{2} Q_n Q_p), \quad (9)$$

$$b_{\alpha n} = \frac{\lambda_\alpha^3}{V} (Q_{\alpha n} - \frac{1}{2} Q_\alpha Q_n) \approx \frac{\lambda_\alpha^3}{V} (Q_{\alpha p} - \frac{1}{2} Q_\alpha Q_p), \quad (10)$$

where again the second approximation neglects the Coulomb interaction and strong-interaction charge dependences. Coulomb effects typically depend on the ratio of the Coulomb energy to the thermal energy $\Gamma_i = Z_i^2 \alpha / a_i T$ [32], where Z_i is the ion charge, α the fine structure constant, and $a_i = (3/4\pi n_i)^{1/3}$ with n_i the ion density. For example, for symmetric nuclear matter (assumed composed only of nucleons) at a density $n = 10^{12}$ g/cm³ and $T = 4$ MeV one has $\Gamma_p = 0.05$, and thus we expect Coulomb effects to be small. However, this should be checked explicitly in future work and Coulomb interactions may be more important when we extend the virial approach to densities where heavy nuclei are present. Note that the choice of λ_α^3 in the last equation (instead of λ^3) is our convention. Below, we will calculate these second virial coefficients from microscopic NN, $N\alpha$ and $\alpha\alpha$ elastic scattering phase shifts.

The pressure P is given by the logarithm of the partition function, which we truncate after second order in the fugacities. In terms of the second virial coefficients, the pressure can be written as

$$\frac{P}{T} = \frac{\log \mathcal{Q}}{V} = \frac{2}{\lambda^3} (z_n + z_p + (z_n^2 + z_p^2) b_n + 2z_p z_n b_{pn}) + \frac{1}{\lambda_\alpha^3} (z_\alpha + z_\alpha^2 b_\alpha + 2z_\alpha (z_n + z_p) b_{\alpha n}). \quad (11)$$

The n , p and α densities follow from derivatives of $\log \mathcal{Q}$ with respect to the chemical potential or the fugacity,

$$n_i = z_i \left(\frac{\partial \log \mathcal{Q}}{\partial z_i} \frac{1}{V} \right)_{V,T}. \quad (12)$$

The resulting n , p and α particle densities are given by

$$n_n = \frac{2}{\lambda^3} (z_n + 2z_n^2 b_n + 2z_p z_n b_{pn} + 8z_\alpha z_n b_{\alpha n}), \quad (13)$$

$$n_p = \frac{2}{\lambda^3} (z_p + 2z_p^2 b_n + 2z_p z_n b_{pn} + 8z_\alpha z_p b_{\alpha n}), \quad (14)$$

$$n_\alpha = \frac{1}{\lambda_\alpha^3} (z_\alpha + 2z_\alpha^2 b_\alpha + 2z_\alpha (z_n + z_p) b_{\alpha n}), \quad (15)$$

where we have used $\lambda^3/\lambda_\alpha^3 = 8$.

These equations provide a parametric form for the virial equation of state that is thermodynamically consistent. For values of z_n and z_p , the alpha fugacity z_α follows from chemical equilibrium $z_\alpha = z_p^2 z_n^2 e^{E_\alpha/T}$ and one can then calculate the pressure P and composition, n_n , n_p and n_α , from Eqs. (11,13-15). The total baryon density n_b is given by

$$n_b = n_n + n_p + 4n_\alpha, \quad (16)$$

and the proton fraction Y_p , the number of protons per baryon, by

$$Y_p = (n_p + 2n_\alpha)/n_b. \quad (17)$$

The dependence of the baryon density and the proton fraction on z_n and z_p can be inverted to yield the virial equation of state in terms of

$$P = P(z_n(n_b, Y_p, T), z_p(n_b, Y_p, T), z_\alpha(z_n, z_p, T), T). \quad (18)$$

Note that these dependences are nonlinear and strongly temperature dependent, mainly due to the $e^{E_\alpha/T}$ term in the chemical equilibrium condition for z_α . In practice, for a given proton fraction, we use Eq. (17) to determine the proton fugacity as a function of the neutron one $z_n(z_p, Y_p, T)$, and generate the virial equation of state in tabular form for a range of z_n . This maintains the thermodynamic consistency of the virial equation of state.

C. Virial Coefficients

We relate the second virial coefficients to the relevant scattering phase shifts. This extends the standard results

for spin-zero particles [29] to include spin and isospin. The virial coefficient is related to the partition function of the two-particles system $\sum_{\text{states}} e^{-E_2/T}$, where the sum is over all two-particle states of energy E_2 . This sum can be converted to an integral over relative momentum k weighted by the density of states. The difference between the density of states of an interacting and a free two-particle system can be expressed in terms of the derivative of the two-body phase shift $d\delta(k)/dk$ [29, 35]. Finally, if one integrates by parts, the virial coefficients can be calculated from an integral over the scattering phase shifts summed over all partial waves with two-body spin S , isospin T , orbital angular momentum L and total angular momentum J allowed by spin statistics.

The virial coefficient b_n describes the interactions in pure neutron matter, and we have

$$b_n(T) = \frac{1}{2^{1/2} \pi T} \int_0^\infty dE e^{-E/2T} \delta_n^{\text{tot}}(E) - 2^{-5/2}. \quad (19)$$

Here, $-2^{-5/2}$ is the free Fermi gas contribution due to the Pauli principle and $\delta_n^{\text{tot}}(E)$ is the sum of the $T = 1$ elastic scattering phase shifts at laboratory energy E . This sum includes a degeneracy factor $(2J + 1)$,

$$\begin{aligned} \delta_n^{\text{tot}}(E) &= \sum_{S,L,J} (2J + 1) \delta_{2S+1L_J}(E) \\ &= \delta_{1S_0} + \delta_{3P_0} + 3 \delta_{3P_1} + 5 \delta_{3P_2} + 5 \delta_{1D_2} + \dots \end{aligned} \quad (20)$$

Here and in the following we have neglected the effects of the mixing parameters due to the tensor force. We expect that their contributions to the second virial coefficients describing spin-averaged observables vanish.

The pn virial coefficient can be decomposed as

$$b_{pn}(T) = b_{\text{nuc}}(T) - b_n(T), \quad (21)$$

where b_{nuc} is the second virial coefficient for symmetric nuclear matter. With b_{pn} and b_n one can describe asymmetric matter with arbitrary proton fraction. For b_{nuc} , the contributions from the deuteron bound state and the scattering continuum are given by

$$\begin{aligned} b_{\text{nuc}}(T) &= \frac{3}{2^{1/2}} (e^{E_d/T} - 1) - 2^{-5/2} \\ &+ \frac{1}{2^{3/2} \pi T} \int_0^\infty dE e^{-E/2T} \delta_{\text{nuc}}^{\text{tot}}(E), \end{aligned} \quad (22)$$

where the term -1 in the deuteron contribution comes from the partial integration (the phase shift at zero energy being π times the number of bound states) and the factor 3 counts the spin-isospin degeneracy of the deuteron. The total phase shift $\delta_{\text{nuc}}^{\text{tot}}(E)$ for nuclear mat-

ter also receives contributions from $T = 0$ states,

$$\begin{aligned}\delta_{\text{nuc}}^{\text{tot}}(E) &= \sum_{S,L,J} (2J+1)(2T+1) \delta_{2S+1L_J}(E) \\ &= 3 \delta_{1S_0} + 3 \delta_{3S_1} + 3 \delta_{1P_1} \\ &\quad + 3 \delta_{3P_0} + 9 \delta_{3P_1} + 15 \delta_{3P_2} + 15 \delta_{1D_2} \\ &\quad + 3 \delta_{3D_1} + 5 \delta_{3D_2} + 7 \delta_{3D_3} + \dots\end{aligned}\quad (23)$$

For spin-zero alpha particles we can directly use the results of [29, 35], which give for the virial coefficient b_α

$$b_\alpha(T) = \frac{2^{1/2}}{\pi T} \int_0^\infty dE e^{-E/2T} \delta_\alpha^{\text{tot}}(E) + 2^{-5/2}, \quad (24)$$

where $+2^{-5/2}$ describes the contribution for a free Bose gas and the total phase shift $\delta_\alpha^{\text{tot}}(E)$ for elastic $\alpha\alpha$ scattering is given by

$$\begin{aligned}\delta_\alpha^{\text{tot}}(E) &= \sum_L (2L+1) \delta_L(E) \\ &= \delta_S + 5 \delta_D + 9 \delta_G + 13 \delta_I + \dots\end{aligned}\quad (25)$$

For the $\alpha\alpha$ virial coefficient and for the following $N\alpha$ virial coefficient, we have not taken into account the effects of inelasticities. For low temperatures, we expect their contributions to be small due to the tight binding of the alpha particle.

Finally, the $N\alpha$ virial coefficient is given by

$$b_{\alpha n}(T) = \left(\frac{5}{4}\right)^{1/2} \frac{1}{\pi T} \int_0^\infty dE e^{-4E/5T} \delta_{\alpha n}^{\text{tot}}(E), \quad (26)$$

with total phase shift $\delta_{\alpha n}^{\text{tot}}(E)$ for $N\alpha$ scattering at nucleon laboratory energy E ,

$$\begin{aligned}\delta_{\alpha n}^{\text{tot}}(E) &= \sum_{L,J} (2J+1) \delta_{L_J}(E) \\ &= 2 \delta_{S_{1/2}} + 2 \delta_{P_{1/2}} + 4 \delta_{P_{3/2}} + 4 \delta_{D_{3/2}} + 6 \delta_{D_{5/2}} \\ &\quad + 6 \delta_{F_{5/2}} + 8 \delta_{F_{7/2}} + \dots\end{aligned}\quad (27)$$

Once the four virial coefficients $b_n(T)$, $b_{pn}(T)$, $b_\alpha(T)$ and $b_{\alpha n}(T)$ have been calculated, the pressure is determined from Eq. (11) using fugacities z_n and z_p that reproduce the desired baryon density n_b and proton fraction Y_p using Eqs. (2,13-17).

D. Entropy and Energy

The entropy S and the energy E can be calculated from the virial equation of state using thermodynamics [11, 35]. The entropy density $s = S/V$ follows from

$$s = \left(\frac{\partial P}{\partial T} \right)_{\mu_i}. \quad (28)$$

Here the temperature derivative is at constant μ_p and μ_n , and thus constant μ_α due to chemical equilibrium. This leads to

$$\begin{aligned}s &= \frac{5P}{2T} - n_n \log z_n - n_p \log z_p - n_\alpha \log z_\alpha \\ &\quad + \frac{2T}{\lambda^3} ((z_n^2 + z_p^2) b'_n + 2z_p z_n b'_{pn}) \\ &\quad + \frac{T}{\lambda_\alpha^3} (z_\alpha^2 b'_\alpha + 2z_\alpha (z_n + z_p) b'_{\alpha n}),\end{aligned}\quad (29)$$

where b'_i denotes the temperature derivative of the second virial coefficients $b'_i(T) = db_i(T)/dT$. The energy density $\epsilon = E/V$ can be calculated from the entropy density by

$$\begin{aligned}\epsilon &= Ts + \sum_{i=n,p,\alpha} n_i \mu_i - P \\ &= \frac{3}{2}P - n_\alpha E_\alpha + \frac{2T^2}{\lambda^3} ((z_n^2 + z_p^2) b'_n + 2z_p z_n b'_{pn}) \\ &\quad + \frac{T^2}{\lambda_\alpha^3} (z_\alpha^2 b'_\alpha + 2z_\alpha (z_n + z_p) b'_{\alpha n}).\end{aligned}\quad (30)$$

We emphasize that the α particle binding-energy contribution $n_\alpha E_\alpha$ is very important for the energy. Finally, the entropy per baryon S/A , energy per baryon E/A and the free energy per baryon F/A are given by

$$\frac{S}{A} = \frac{s}{n_b}, \quad \frac{E}{A} = \frac{\epsilon}{n_b} \quad \text{and} \quad \frac{F}{A} = \frac{f}{n_b}, \quad (31)$$

with the free energy density $f = \epsilon - Ts$.

III. RESULTS

In this section, we present results for the second virial coefficients, the equation of state and the composition, as well as the entropy, energy and symmetry energy.

A. Virial Coefficients

We first calculate the NN virial coefficients. We take the NN phase shifts from the Nijmegen partial wave analysis [36] and use pn phase shifts for both $T = 0$ and $T = 1$ states. We thus neglect the Coulomb interaction and strong-interaction charge dependences. In general, we expect that their effects on interaction energies are small. All partial waves with $L \leq 2$ are included and we have checked that higher contributions are negligible for the temperatures of interest. The resulting total phase shifts for neutron and nuclear matter are shown in Fig. 1.

For neutron matter, we observe that $\delta_n^{\text{tot}}(E)$ is approximately energy-independent over a wide range. The decrease of the 1S_0 phase shift with increasing energy is compensated by the contributions from higher angular momenta. As a result, the neutron virial coefficient b_n

TABLE I: NN virial coefficients for different temperatures. In addition to the full results, we also give the virial coefficients calculated only from the large S-wave scattering lengths ($a_{1S_0} = -23.768$ fm, $a_{3S_1} = 5.420$ fm) and the deuteron binding energy.

T [MeV]	b_n full	b_n only a_s	$T b'_n$ full	b_{pn} full	b_{pn} only a_s, E_d	$T b'_{pn}$ full	b_{nuc} full	b_{nuc} only a_s, E_d	$T b'_{nuc}$ full
1	0.288	0.357	0.032	19.4	19.5	-43.8	19.7	19.8	-43.8
2	0.303	0.400	0.012	6.10	6.24	-7.39	6.40	6.64	-7.38
3	0.306	0.421	0.005	4.01	4.19	-3.54	4.31	4.61	-3.53
4	0.307	0.434	0.002	3.19	3.40	-2.30	3.50	3.83	-2.30
5	0.308	0.443	0.002	2.74	2.98	-1.73	3.05	3.43	-1.72
6	0.308	0.450	0.003	2.46	2.72	-1.40	2.77	3.18	-1.39
7	0.308	0.456	0.004	2.26	2.54	-1.18	2.57	3.00	-1.18
8	0.309	0.460	0.006	2.11	2.42	-1.04	2.42	2.88	-1.03
9	0.310	0.464	0.008	2.00	2.32	-0.93	2.31	2.79	-0.92
10	0.311	0.467	0.010	1.91	2.24	-0.85	2.22	2.71	-0.84

will be approximately temperature-independent. In contrast, $\delta_{nuc}^{tot}(E)$ decreases with increasing energy due to the decrease in the additional 3S_1 phase shift. This behavior of the total phase, along with the strong temperature dependence of the deuteron contribution $e^{E_d/T}$, will lead to second virial coefficients b_{pn} and b_{nuc} that decrease rapidly with temperature.

In Table I, we give our results for the NN virial coefficients $b_n(T)$, $b_{pn}(T)$ and $b_{nuc}(T)$, as well as their derivatives $T b'_i(T)$. As expected, the NN virial coefficients are dominated by the large S-wave scattering lengths and deuteron physics, but effective range and higher partial wave contributions are significant even for these relatively low temperatures. We also emphasize that the effects of the low-energy 1S_0 resonance encoded in b_n become more important in neutron-rich matter.

Next, we calculate the $N\alpha$ virial coefficient. We neglect Coulomb interactions and thus use neutron-alpha

phase shifts up to $L \leq 3$. For laboratory energies $E < 20$ MeV, we take the simple phase shift fits of Arndt and Roper [37], which are constrained by scattering data over these energies. We extrapolate to higher energies using microscopic phase shift predictions based on optical model calculations by Amos and Karataglidis [38]. Note for these calculations we assume $|\delta_{L,J}| < \pi$. Since we neglect the effects of inelasticities, we take the real part of the predicted phase shifts of Amos and Karataglidis. The differences between the real part and the absolute value of the phase shifts are generally small over the relevant energies. The neutron-alpha elastic scattering phase shifts are shown in Fig. 2. The $P_{3/2}$ wave has a resonance at $E \approx 1$ MeV with $P_{3/2}$ scattering length $a_{P_{3/2}} = -62.95$ fm³ [39], and therefore will be the most important contribution to the $N\alpha$ virial coefficient. The other partial waves are not resonant at low energies. Our results for the $N\alpha$ virial coefficients are listed in Table II. We expect that more accurate high-energy phases will only slightly change our results for $b_{\alpha n}$ for temperatures $T > 5$ MeV.

Finally, we show the phase shifts for elastic $\alpha\alpha$ scattering in Fig. 3. The low-energy phase shifts are taken from Afzal *et al.* [40] and the phase shifts for energies between 30 MeV and 70 MeV are from Bacher *et al.* [41]. The phase shifts display a pronounced 0^+ resonance at very low energies that corresponds to the ^8Be ground state. This resonance is crucial for ^4He burning in red giant stars. Just below 35 MeV there are also two very close 2^+ resonances (they are both at $E \approx 34$ MeV in Fig. 3) and in general the phase shifts become large at high energies. We include all $\alpha\alpha$ phases with $L \leq 6$ for the calculation of b_α , where we make the following approximations. First, we neglect the Coulomb interaction. We also neglect inelastic channels. Fortunately, the α particle is so tightly bound that important inelastic contributions do not arise until relatively high energies. Finally, we truncate the integration for b_α at 70 MeV (the extent of the data). Our results for the $\alpha\alpha$ virial coefficients are given in Table II. As for the NN virial coefficients, $b_{\alpha n}$ and b_α are dominated by the relevant low-energy resonances, but

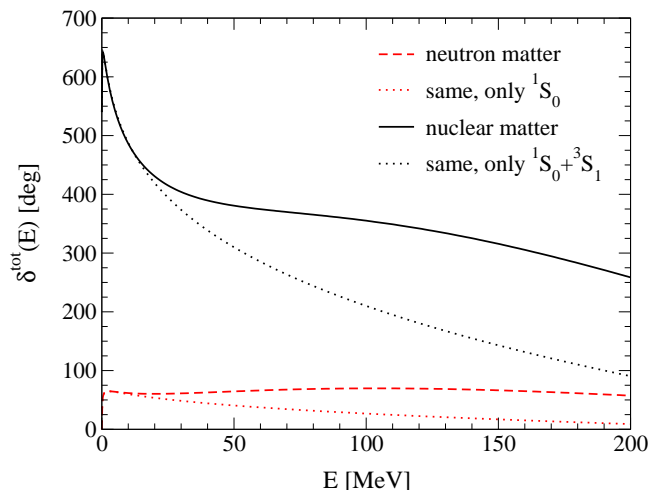


FIG. 1: (Color online) The total phase shift $\delta_n^{tot}(E)$ for neutron matter and $\delta_{nuc}^{tot}(E)$ for nuclear matter versus laboratory energy E . For reference, we also show the contributions from only the S-wave phase shifts.

TABLE II: $N\alpha$ and $\alpha\alpha$ virial coefficients for different temperatures. In addition to the full results, we also give the virial coefficients calculated only from the dominant low-energy resonances ($P_{3/2}$ -wave for $N\alpha$, and S- and D-waves for $\alpha\alpha$).

T [MeV]	$b_{\alpha n}$ full	$b_{\alpha n}$ only $P_{3/2}$ -wave	$T b'_{\alpha n}$ full	b_{α} full	b_{α} only S- and D-waves	$T b'_{\alpha}$ full
1	1.51	1.73	1.21	2.55	2.55	1.59
2	2.26	2.48	0.90	4.12	4.00	2.95
3	2.57	2.78	0.63	5.64	5.07	4.81
4	2.73	2.91	0.44	7.44	6.02	7.90
5	2.81	2.97	0.32	9.57	7.01	11.3
6	2.86	2.99	0.23	11.9	8.05	14.3
7	2.89	2.99	0.18	14.3	9.08	16.3
8	2.92	2.98	0.15	16.5	10.0	17.3
9	2.93	2.96	0.14	18.6	10.9	17.5
10	2.95	2.93	0.13	20.4	11.7	17.0

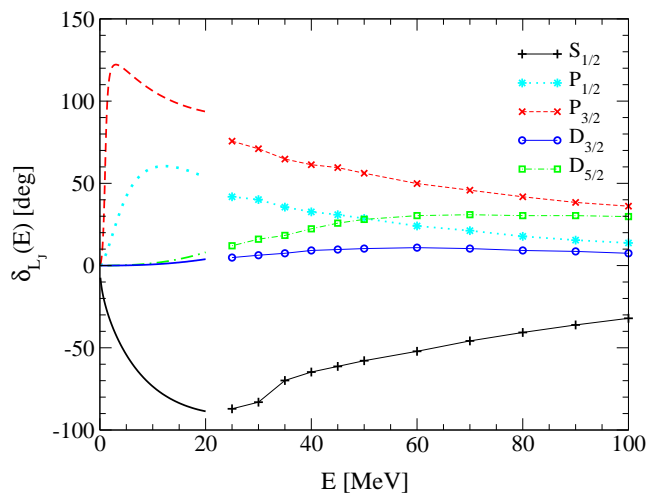


FIG. 2: (Color online) The phase shifts for elastic neutron-alpha scattering $\delta_{L_j}(E)$ versus laboratory energy E . As discussed in the text, the solid lines are from Arndt and Roper [37] and the symbols are from Amos and Karataglidis [38]. For clarity, we do not show the F-waves included in our results for $b_{\alpha n}$.

b_{α} receives important contributions from higher angular momentum resonances for $T > 5$ MeV.

In addition to the values for the NN, $N\alpha$ and $\alpha\alpha$ virial coefficients given in Tables I and II for $T \leq 10$ MeV, we extend our results to higher temperatures in Table III. We list these results in a separate table, as our approximations, mainly the neglect of inelastic channels and the truncation of the integration over the phase shifts at the extent of the data, may be more severe.

B. Composition

We now discuss the α particle concentration. The α mass fraction is given by $x_{\alpha} = 4n_{\alpha}/n_b$. In Fig. 4, we show

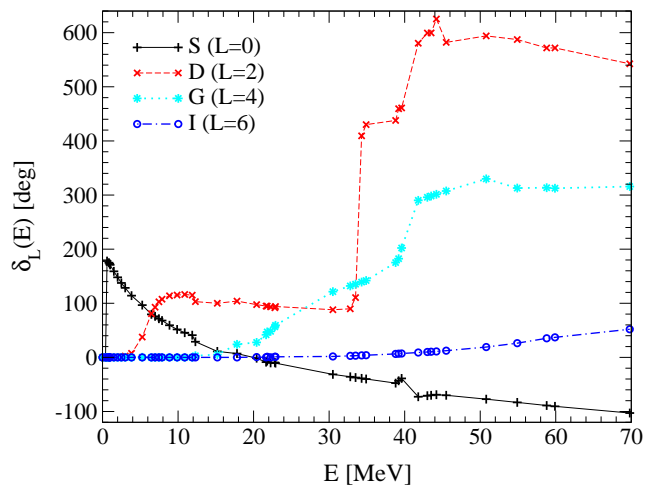


FIG. 3: (Color online) The phase shifts for elastic $\alpha\alpha$ scattering $\delta_L(E)$ versus laboratory energy E . As discussed in the text, the phase shifts are taken from Afzal *et al.* [40] and from Bacher *et al.* [41].

x_{α} for a temperature $T = 4$ MeV and proton fraction $Y_p = 1/2$ with various values of the virial coefficients. The largest α particle concentration results for a free n, p, α gas, where all $b_i = 0$. Including nucleonic interactions $b_n, b_{pn}, b_{nuc} \neq 0$, but still keeping $b_{\alpha}, b_{\alpha n} = 0$ reduces x_{α} significantly. This is because the attractive nuclear interactions reduce the nucleon chemical potential, and this leads to a reduction of x_{α} . Including also $b_{\alpha n} \neq 0$ increases the α mass fraction, but x_{α} is still smaller than its free value. The latter effect is dominated by the low-energy $N\alpha$ resonance. Finally, including $b_{\alpha} \neq 0$ only increases x_{α} by a very small amount. Therefore, in general, NN virial coefficients are expected to be most important, while the $N\alpha$ virial coefficient leads to small changes, and b_{α} is least important. This hierarchy is because typically $n_p + n_n > n_{\alpha}$.

The LS model excludes nucleons from the volume occupied by alpha particles. Although this is a prescription,

TABLE III: NN, $N\alpha$ and $\alpha\alpha$ virial coefficients for higher temperatures. Note that inelasticities are neglected and that the integration over the $\alpha\alpha$ elastic scattering phase shifts is truncated at $E \leq 70$ MeV.

T [MeV]	b_n full	$T b'_n$ full	b_{pn} full	$T b'_{pn}$ full	b_{nuc} full	$T b'_{nuc}$ full	$b_{\alpha n}$ full	$T b'_{\alpha n}$ full	b_α full	$T b'_\alpha$ full
12	0.313	0.013	1.76	-0.73	2.08	-0.72	2.97	0.12	23.3	14.7
14	0.315	0.014	1.66	-0.65	1.97	-0.64	2.98	0.10	25.4	11.7
16	0.317	0.014	1.57	-0.59	1.89	-0.58	3.00	0.07	26.7	8.48
18	0.319	0.013	1.51	-0.55	1.82	-0.54	3.00	0.02	27.5	5.44
20	0.320	0.011	1.45	-0.52	1.77	-0.51	3.00	-0.04	28.0	2.69

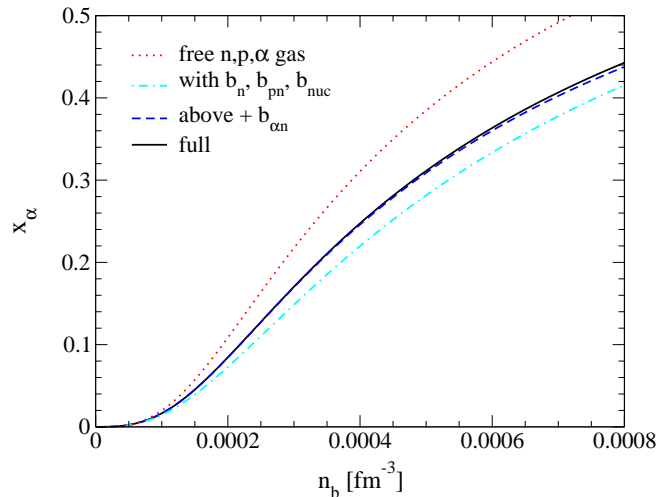


FIG. 4: (Color online) The α mass fraction x_α versus baryon density n_b for $T = 4$ MeV, $Y_p = 1/2$ and various values of the virial coefficients, as explained in the text. The fugacities are small over this density range $z_n = z_p < 0.05$ and $z_\alpha < 0.004$.

it leads to an α mass fraction that vanishes in the high-density limit [42]. The effects of the excluded volume are small at low densities. However, the excluded volume corresponds to a repulsive $N\alpha$ interaction that reduces the α particle concentration. In contrast, the neutron-alpha resonance and the attractive total phase shift leads to an attractive $N\alpha$ interaction in the virial expansion. As a result, the α mass fraction increases, as shown in Fig. 4. Therefore, the excluded volume alone gives the wrong sign for $N\alpha$ interactions in the low-density limit, but we caution that the effects of the excluded volume and the $N\alpha$ virial coefficient may be small at very low densities.

The third virial coefficient $b_{nuc}^{(3)}$ can be used to make a simple error estimate of neglected terms in the virial expansion. From the above conclusion, we expect $b_{nuc}^{(3)}$ to be the most important of the third virial coefficients, and we therefore take into account only $b_{nuc}^{(3)}$ in this estimate. For simplicity, we consider symmetric nuclear matter with $z_p = z_n = z$, for which the virial equation of

state, Eqs. (11,13-15), including $b_{nuc}^{(3)}$ reads

$$\frac{P}{T} = \frac{4}{\lambda^3} (z + z^2 b_{nuc} + z^3 b_{nuc}^{(3)}) + \frac{1}{\lambda_\alpha^3} (z_\alpha + z_\alpha^2 b_\alpha + 4z_\alpha z b_{\alpha n}), \quad (32)$$

$$n = n_p + n_n = \frac{4}{\lambda^3} (z + 2z^2 b_{nuc} + 3z^3 b_{nuc}^{(3)} + 8z_\alpha z b_{\alpha n}), \quad (33)$$

$$n_\alpha = \frac{1}{\lambda_\alpha^3} (z_\alpha + 2z_\alpha^2 b_\alpha + 4z_\alpha z b_{\alpha n}). \quad (34)$$

In Fig. 5, we again plot the α mass fraction. The solid line is our previous result with $b_{nuc}^{(3)} = 0$. We also give approximate error bands by considering $b_{nuc}^{(3)} = 10$ (which gives a lower x_α) and $b_{nuc}^{(3)} = -10$. This estimates the error only from the effect of a typical neglected term in the virial expansion. Our estimate $|b_{nuc}^{(3)}| < 10$ is somewhat arbitrary, as it is based on the observation that all second virial coefficients are comfortably less than 10 for $T = 4$ MeV. We see from Fig. 5 that the resulting error band is small. *Therefore, our virial expansion makes a model-independent prediction for the α particle concentration.* We also contrast our results in Fig. 5 to the x_α predicted by two phenomenological equations of state. The Lattimer-Swesty (LS) equation of state [26] is based on an extended liquid drop model and is almost universally used in modern supernova simulations. The LS model predicts too few alpha particles over the densities where the virial equation of state is applicable. Alternatively, the Shen-Toki-Oyamatsu-Sumiyoshi (Shen) equation of state [27] is based on an approximate Thomas Fermi calculation using a relativistic mean-field interaction. The Shen equation of state predicts slightly too high values for x_α at this temperature.

It is a simple matter to apply the virial equation of state to different proton fractions and temperatures. In Fig. 6, we show how the α particle concentration decreases with decreasing proton fraction Y_p for $T = 4$ MeV. In addition, we give x_α for $Y_p = 1/2$ and a range of temperatures $T = 2, 4$ and 8 MeV in Fig. 7. At the lowest temperature $T = 2$ MeV, x_α rises rapidly at low densities where the virial coefficients make only small contributions. Therefore the error band is very small. The error band becomes more important for $T = 8$ MeV.

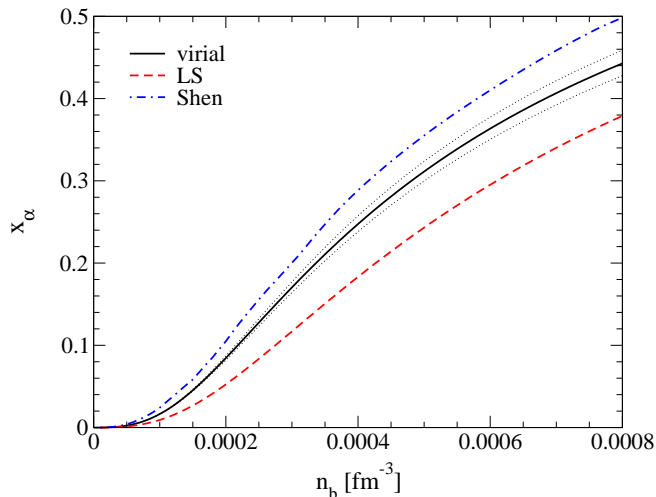


FIG. 5: (Color online) The α mass fraction x_α versus baryon density n_b for $T = 4$ MeV and $Y_p = 1/2$. The dotted error band for the virial equation of state is based on an estimate of a neglected third virial coefficient $b_{\text{nuc}}^{(3)} = \pm 10$. Also shown are results for the LS [26] and Shen [27] equations of state.

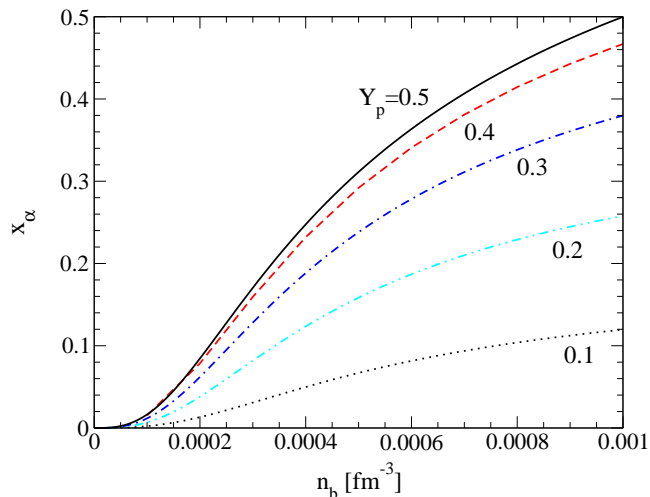


FIG. 6: (Color online) The α mass fraction x_α versus baryon density n_b for $T = 4$ MeV and proton fractions $Y_p = 0.1, 0.2, 0.3, 0.4$ and 0.5 . For the lowest proton fraction $Y_p = 0.1$, the fugacities are $z_n < 0.2$, $z_p < 0.005$ and $z_\alpha < 0.001$ over this density range.

The LS equation of state is seen to significantly underestimate x_α at all three temperatures. This may be due to a simple oversight in the published version [26] of the LS equation of state. Lattimer and Swesty include the neutron-proton mass difference in the proton chemical potential, but do not appear to include twice this difference in the alpha chemical potential. In contrast, the Shen equation of state is close to our virial results at low densities. However, both LS and Shen equations of state predict too few α particles at high temperatures $T > 10$ MeV. This can be clearly seen from the α mass fraction shown in Fig. 8 for $T = 20$ MeV. The differ-

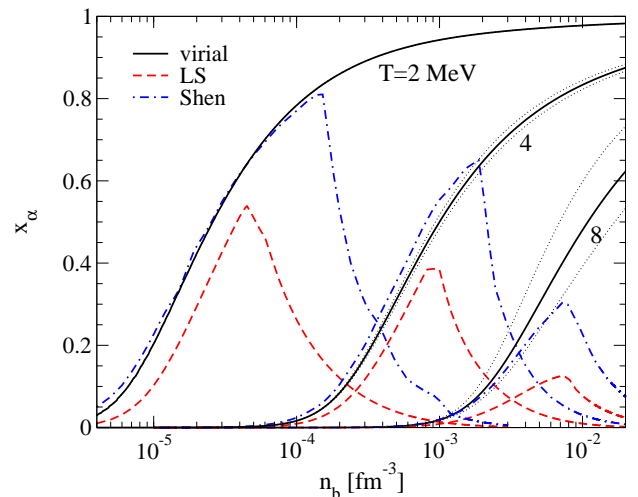


FIG. 7: (Color online) The α mass fraction x_α versus baryon density n_b for $T = 2, 4$ and 8 MeV and $Y_p = 1/2$. The dotted error bands for the virial equation of state are based on an estimate of a neglected third virial coefficient $b_{\text{nuc}}^{(3)} = \pm 10$. Note that for $T = 2$ MeV the error band is very small. Also shown are results for the LS [26] and Shen [27] equations of state. Over this density range, the fugacities are $z_n = z_p < 0.03, 0.10, 0.16$ and $z_\alpha < 0.27, 0.09, 0.03$ for $T = 2, 4, 8$ MeV.

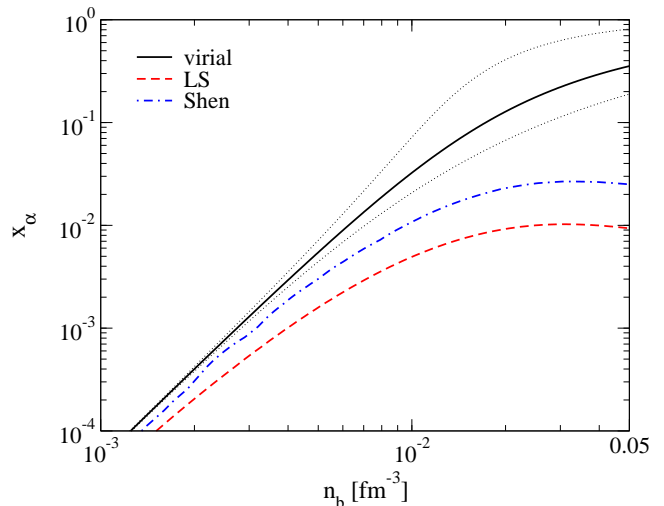


FIG. 8: (Color online) The α mass fraction x_α versus baryon density n_b for $T = 20$ MeV and $Y_p = 1/2$. The dotted error bands for the virial equation of state are based on an estimate of a neglected third virial coefficient $b_{\text{nuc}}^{(3)} = \pm 10$. Also shown are results for the LS [26] and Shen [27] equations of state. Over this density range, the fugacities are $z_n = z_p < 0.21$ and $z_\alpha < 0.07$.

ences of the LS and Shen equations of state at the higher densities shown for $T = 20$ MeV in Fig. 8 are due to the differences in the symmetry energy [43].

Both phenomenological equations of state shown in Fig. 7 give α particle concentrations that first increase with density and then rapidly decrease. This decrease is due to the formation of heavy nuclei. Heavy nuclei are not included in our first studies. We will extend the

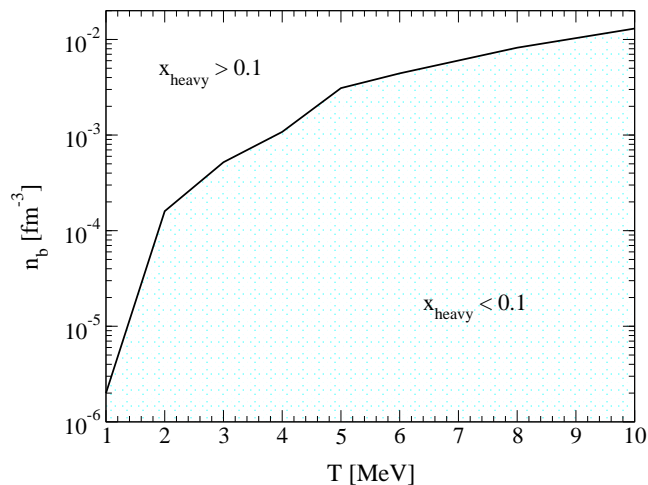


FIG. 9: (Color online) The threshold baryon density n_b above which the Shen equation of state [27] predicts a heavy nuclei mass fraction larger than 10%. This figure is for $Y_p = 1/2$.

virial formalism to include heavy nuclei in future work. Therefore, our virial results are currently limited to lower densities, where one does not expect large contributions from heavy nuclei. In Fig. 9, we plot the density above which the Shen equation of state has a heavy nuclei mass fraction larger than 10%. This provides an estimate for the range of validity of the virial n, p, α equation of state. For this estimate we have considered the Shen instead of the LS model due to the LS error in x_α .

C. Pressure

Next, we present our results for the pressure. In Fig. 10, we plot the pressure of symmetric nuclear matter for $T = 10$ MeV. The formation of α particles reduces the total number of particles in the system, and this significantly lowers the pressure. For comparison, we also show in Fig. 10 the microscopic Fermi hypernetted-chain (FHNC) equation of state of Friedman and Pandharipande [13]. The latter calculation is based on a variational wave function with only two-nucleon correlations. However, the model-independent virial equation of state shows that there are large α concentrations in this density regime. For example, at the threshold density of $n_b = 0.013 \text{ fm}^{-3}$ (from Fig. 9) we have $x_\alpha = 0.40$. Microscopic calculations may require wave functions with four-nucleon correlations to accurately describe these α particle contributions. *This suggests that all present microscopic variational or Brueckner equations of state are incomplete in their description of low-density nuclear matter.* In Fig. 10, we also give the pressure for densities beyond the threshold density of Fig. 9 in order to compare virial and FHNC results, which both omit the formation of heavy nuclei.

The error band in Fig. 10 is again estimated from a

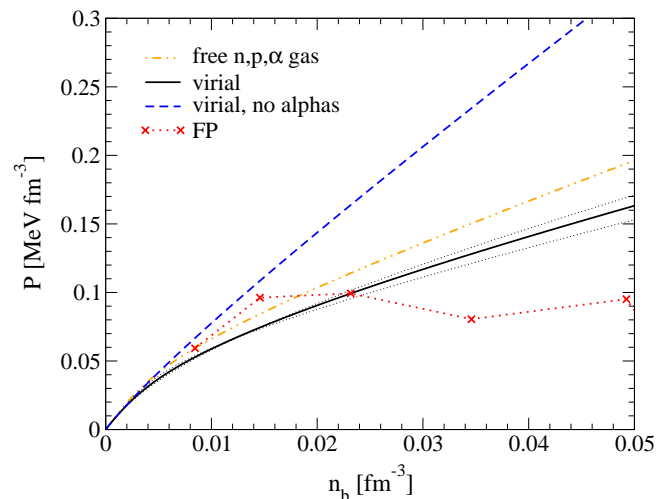


FIG. 10: (Color online) The pressure P of symmetric nuclear matter versus baryon density n_b for $T = 10$ MeV. The dotted error band for the virial equation of state is based on an estimate of a neglected third virial coefficient $b_{\text{nuc}}^{(3)} = \pm 10$. Also shown are virial results without α particles ($z_\alpha = 0$) and the microscopic FHNC results of Friedman and Pandharipande (FP) [13]. The effects of interactions are illustrated by comparing to the pressure of a free gas of nucleons and alpha particles. Over this density range, the fugacities are $z_n = z_p < 0.21$ (< 0.51 without alphas, < 0.32 for the free gas) and $z_\alpha < 0.04$ (< 0.17 free gas).

neglected third virial coefficient $b_{\text{nuc}}^{(3)} = \pm 10$. For the pressure, this involves a cancellation. Increasing $b_{\text{nuc}}^{(3)}$ decreases the nucleonic contribution to the pressure due to the additional attractive interaction between nucleons. However, a larger $b_{\text{nuc}}^{(3)}$ also reduces the formation of α particles (due to a lower alpha chemical potential), and this acts to increase the total pressure. Therefore, a positive $b_{\text{nuc}}^{(3)}$ reduces the pressure at very low densities, but then leads to a larger pressure with increasing density.

In Fig. 11, we show our results for the pressure of symmetric nuclear matter for $T = 4$ MeV in comparison to the phenomenological LS and Shen equations of state. The pressure given in Fig. 11 also includes the contribution of an electron and photon gas as in Appendix C of [26]. We find the pressures given by the virial equation of state and the phenomenological models agree well.

In a separate paper [6], we have demonstrated that the equation of state of low-density neutron matter scales to a very good approximation. Table I shows that the neutron virial coefficient $b_n(T)$ is practically independent of the temperature. If all virial coefficients are temperature independent, and provided the condition for chemical equilibrium does not introduce a strong temperature dependence through $z_\alpha(z_n, z_p, T)$, then the power series in the fugacity for the pressure and the baryon density will have no explicit temperature dependence. In this

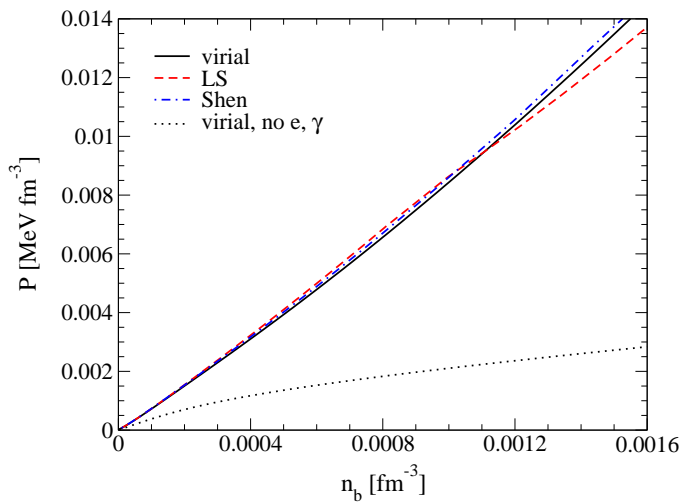


FIG. 11: (Color online) The pressure P of symmetric nuclear matter versus baryon density n_b for $T = 4$ MeV. As discussed in the text, these results include the contribution of an electron and photon gas, and we also show the virial pressure without this contribution. In addition, we give the results of the LS [26] and Shen [27] equations of state. Over this density range, the fugacities are $z_n = z_p < 0.06$ and $z_\alpha < 0.01$.

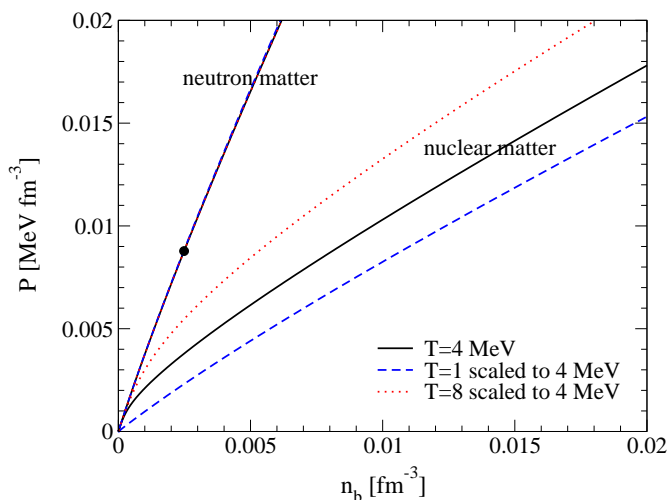


FIG. 12: (Color online) The pressure P of pure neutron matter and of symmetric nuclear matter calculated for $T = 1, 4$ and 8 MeV and scaled to a temperature of $T' = 4$ MeV (for details see text). The circle indicates where $z_n = 0.5$ for pure neutron matter. For symmetric nuclear matter, the fugacities are $z_n = z_p < 0.10$ and $z_\alpha < 0.09$ over this density range.

case, the pressure will scale as

$$P(n_b, T) = T^{5/2} f(n_b/T^{3/2}), \quad (35)$$

where $f(x)$ is some function of $n_b/T^{3/2}$. If this scaling relation holds, one can predict the pressure $P(n_b, T')$ at a new temperature T' from the original $P(n_b, T)$ through

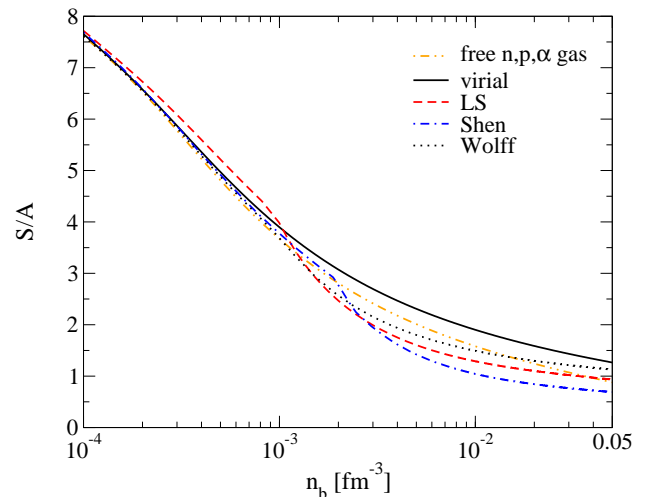


FIG. 13: (Color online) The entropy per baryon S/A versus baryon density n_b for $T = 4$ MeV and $Y_p = 1/2$. As discussed in the text, these results include the contribution of an electron and photon gas. Also shown are results for the LS [26], Shen [27] and the Wolff [44] equations of state. The effects of interactions are illustrated by comparing to the entropy of a free gas of nucleons and alpha particles. Over this density range, the fugacities are $z_n = z_p < 0.11$ (< 0.17 for the free gas) and $z_\alpha < 0.17$ (< 0.81 free gas).

$$P(n_b, T') = \left(\frac{T'}{T}\right)^{5/2} P(\tilde{n}_b, T), \quad (36)$$

with $n_b = (T'/T)^{3/2} \tilde{n}_b$.

We study this scaling symmetry in Fig. 12, where we have used Eq. (36) to predict the pressure of neutron matter for $T' = 4$ MeV from virial pressures calculated for $T = 1$ and 8 MeV. The agreement with the unscaled $T = 4$ MeV virial pressure is excellent. This demonstrates that low-density neutron matter scales, even when interactions are included. Fig. 12 also shows scaled pressures of symmetric nuclear matter for $T' = 4$ MeV using $T = 1$ and 8 MeV results as input. These scaled pressures do not agree with the $T = 4$ MeV virial pressure. Therefore, nuclear matter does not scale, which is due to clustering and mainly comes as a result of the strong temperature dependence of z_α and x_α .

D. Entropy and Energy

The entropy per baryon S/A of symmetric nuclear matter is shown for $T = 4$ MeV in Fig. 13. Here, our virial calculation again includes the entropy of an electron and photon gas as in Appendix C of [26]. The entropy is clearly seen to reflect the composition. At low densities, the LS entropy is above the other calculations because of the low α mass fraction in the LS model. At high

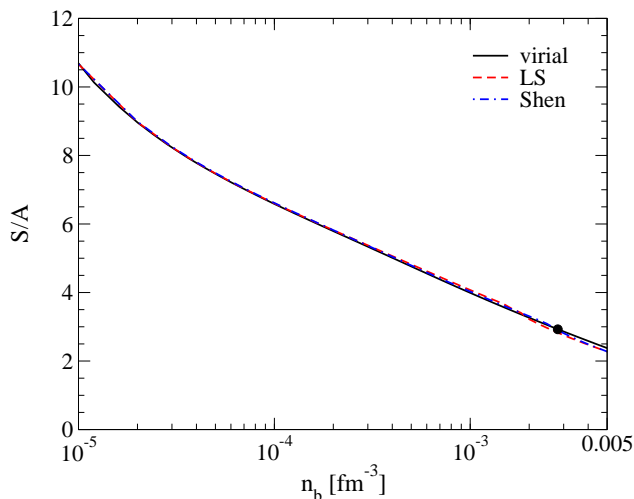


FIG. 14: (Color online) The entropy per baryon S/A versus baryon density n_b for $T = 4$ MeV and $Y_p = 0.05$. As discussed in the text, these results include the contribution of an electron and photon gas. Also shown are results for the LS [26] and the Shen [27] equations of state. The circle indicates where $z_n = 0.5$ ($z_p = 0.002$ and $z_\alpha = 0.001$).

densities, the entropy in the phenomenological models is below our virial result due to the formation of heavy nuclei. This deviation coincides with the threshold density of Fig. 9. In Fig. 13, we also show the entropy per baryon for the Wolff equation of state [44], to give a measure for the model dependence of the onset of heavy nuclei. The entropy per baryon for extremely neutron-rich matter $Y_p = 0.05$ is shown in Fig. 14. Now there is very little change in composition, and thus good agreement between the virial and phenomenological results.

In addition to the entropy, we show our results for the energy per baryon E/A in Fig. 15. In the limit of very low density, the energy reduces to the kinetic energy of an ideal classical gas $3T/2$. Therefore, we have subtracted $3T/2$ from E/A in Fig. 15, in order to clearly show the interaction effects. We find that the energy per baryon for pure neutron matter is somewhat below $3T/2$ due to the attractive nuclear interactions. Our neutron matter results are in excellent agreement with the scaling law for the energy density $\epsilon = 3/2P$, which follows from Eq. (30) when the virial coefficients are temperature independent, as is the case for neutron matter with $b'_n \approx 0$. In contrast, E/A for symmetric nuclear matter drops very rapidly with increasing density. This reflects the large binding energy as α particles form. As can be seen from Fig. 15, this drop becomes more rapid for lower temperatures. We therefore expect that the inclusion of heavy nuclei, or many-nucleon correlations, are necessary to obtain a constant energy per particle $E/A \approx -16$ MeV for $T = 0$ nuclear matter at subsaturation densities.

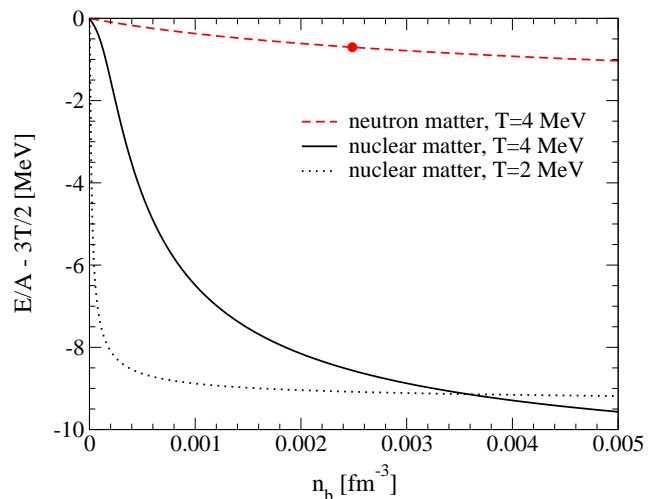


FIG. 15: (Color online) The energy per baryon E/A versus baryon density n_b for $T = 4$ MeV (and also $T = 2$ MeV (dotted) for nuclear matter). In order to clearly show the interaction effects we have subtracted the free kinetic energy $3T/2$ from all curves. The circle indicates where $z_n = 0.5$ for pure neutron matter. For symmetric nuclear matter, the fugacities are $z_n = z_p < 0.08, 0.02$ and $z_\alpha < 0.03, 0.11$ for $T = 4$ and 2 MeV respectively.

E. Symmetry Energy

The symmetry energy S_E characterizes how the energy rises as one moves away from equal numbers of neutrons and protons,

$$S_E = \frac{1}{8} \frac{\partial^2 E}{\partial Y_p^2} \bigg|_{Y_p=1/2}. \quad (37)$$

We evaluate the second derivative of the energy per baryon with respect to the proton fraction numerically. Fig. 16 shows the symmetry energy for $T = 4$ MeV. At very low density, S_E rises slowly with density. To lowest order in the density and neglecting α particles, the symmetry energy is given by

$$S_E \approx \frac{3}{8} T \lambda^3 n_b (b_{pn} - 2Tb'_{pn}/3 - b_n + 2Tb'_n/3). \quad (38)$$

Then, as α particles form, S_E rises much faster with density. As a result of clustering, the symmetry energy is large even at a very small fraction of saturation density. This is analogous to the observed behavior for the energy.

We also show in Fig. 16 the symmetry free energy S_F defined as

$$S_F = \frac{1}{8} \frac{\partial^2 F}{\partial Y_p^2} \bigg|_{Y_p=1/2}. \quad (39)$$

To lowest order in the density and neglecting α particles, the symmetry free energy is given by

$$S_F \approx \frac{T}{2} + \frac{1}{4} T \lambda^3 n_b (b_{pn} - b_n), \quad (40)$$

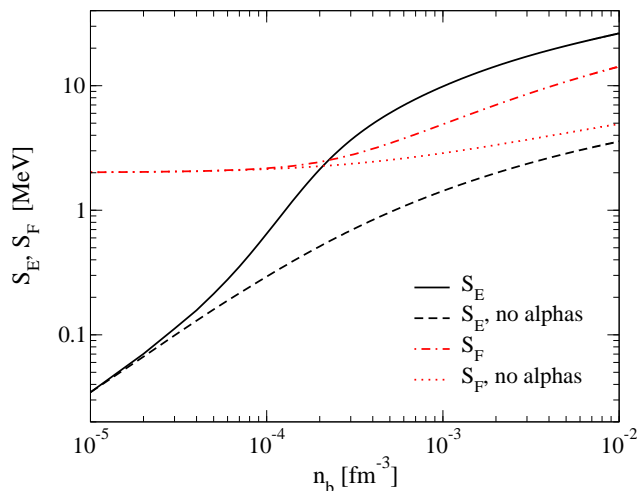


FIG. 16: (Color online) The symmetry energy S_E and the symmetry free energy S_F versus baryon density n_b for $T = 4$ MeV. Also shown are virial results without α particles ($z_\alpha = 0$). Over this density range, the fugacities are $z_n = z_p < 0.09$ (< 0.37 without alphas) and $z_\alpha < 0.06$.

where the $T/2$ term is from the entropy of mixing in the free energy density. Again, as α particles form, we find in Fig. 16 that S_F increases rapidly with density.

Finally, the temperature dependence of the symmetry energy is shown in Fig. 17 for $T = 2, 4$ and 8 MeV. The lower the temperature, the more rapidly S_E rises with density. We conclude that, in the thermodynamic limit, the symmetry energy is large at low densities due to cluster formation.

Isospin observables in asymmetric heavy-ion collisions, such as the N/Z ratio of emitted fragments, are often analyzed with semiclassical simulations, where nucleons move in isospin-dependent mean fields and undergo two-nucleon collisions. The isospin-dependent mean-field implies a certain symmetry energy. The density dependence of this symmetry energy can be adjusted to improve agreement with the data, e.g., see [45]. This phenomenological symmetry energy at low densities is in general much smaller than our virial S_E . This is because the symmetry energy in the virial expansion includes the contributions of clusters with high central densities even at low baryon density. The relation between S_E and the symmetry energy of mean-field models for single nuclei should therefore be investigated in future work.

IV. CONCLUSIONS

We have presented the equation of state of low-density nuclear matter using the model-independent virial expansion. The virial equation of state is thermodynamically consistent and was calculated directly from binding energies and scattering phase shifts, without the need of a nuclear interaction model or nuclear wave functions.

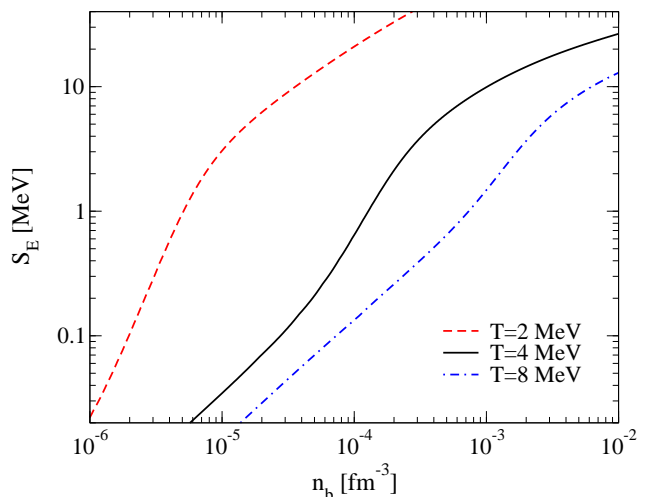


FIG. 17: (Color online) The symmetry energy S_E versus baryon density n_b for $T = 2, 4$ and 8 MeV. Over this density range, the fugacities are $z_n = z_p < 0.02, 0.09, 0.13$ and $z_\alpha < 0.18, 0.06, 0.01$ for $T = 2, 4, 8$ MeV.

Therefore, our results provide a benchmark for all microscopic or phenomenological equations of state at low densities. The virial equation of state can also be used to constrain models that extend to higher densities. In some cases, our virial results may be used to constrain model parameters or functional forms for model interactions. In other cases, more extensive modifications of the phenomenological equations of state may be necessary in order to reproduce the virial low-density limit.

Tightly bound nuclei can lead to unnaturally large bound state contributions to the higher-order virial coefficients. Therefore, we have considered a gas of nucleons and alpha particles to explicitly take into account the large α particle binding energy. This leads to a larger radius of convergence compared to a nucleonic virial expansion. We have calculated the second virial coefficients for NN, $N\alpha$ and $\alpha\alpha$ interactions directly from the relevant binding energies and scattering phase shifts. For the temperatures of interest, the virial coefficients are dominated by the low-energy bound states and resonances, but higher partial wave contributions are significant.

We have found that the second virial coefficient for neutron matter b_n is approximately temperature-independent, which leads to an approximate scaling symmetry of pure neutron matter. The second virial coefficients for nuclear matter b_{pn} and b_{nuc} decrease with temperature, and as a result nuclear matter does not scale. The second virial coefficient for $N\alpha$ interactions $b_{\alpha n}$ is well approximated by the resonant $P_{3/2}$ contribution. This holds over a wide range of energies due to a cancellation among the additional partial waves. The second virial coefficient for $\alpha\alpha$ interactions b_α increases with temperature, as the $\alpha\alpha$ phase shifts become large at higher energies. The inclusion of the Coulomb interac-

tion for the virial coefficients, and the proper treatment of inelasticities and mixing parameters (due to the tensor force) are important topics for future improvements.

We have used the virial coefficients to make model-independent predictions for a variety of properties of nuclear matter over a range of densities, temperatures and composition. The resulting α particle concentration disagrees with all equations of state currently used in supernova simulations. The contributions from low-energy resonances show most prominently in the composition of low-density nuclear matter.

The effects of the second virial coefficients follows a natural hierarchy, with the NN virial coefficients being more important than the $N\alpha$ virial coefficient, and the $\alpha\alpha$ virial coefficient leading to very small changes. We have used this hierarchy to make simple error estimates by studying the effects of a neglected third virial coefficient $b_{\text{nuc}}^{(3)} = \pm 10$. The resulting error bands are small. Detailed investigations of the effects of omitted higher virial coefficients, as well as the effects of heavy nuclei will be the topic of separate studies. For a better error estimate, it is important to also have a reliable calculation of the third virial coefficients, which could, e.g., come from a calculation in the effective field theory for halo nuclei [46]. Furthermore, these error estimates can also help clarify the domain of validity of the virial expansion.

The physics of nuclear matter is very different from neutron matter due to clustering. As the density increases, α particles form and this leads to a significant reduction of the pressure of low-density nuclear matter. Similarly, clustering increases the binding energy and it

reduces the entropy, which reflects the number of particles in the system. As the density increases further, heavier nuclei and larger clusters form, and α particles become less important. In fact, the breakdown of the virial expansion for nuclear matter is due to the formation of heavy nuclei, which is reached before the nucleon fugacities become large. In nuclear matter at $T = 0$, we expect that one has to explicitly include heavy nuclei, or many-nucleon correlations, to obtain a constant energy per baryon $E/A \approx -16$ MeV and a constant symmetry energy at low densities. These virial results greatly improve our conceptual understanding of nuclear matter at subsaturation densities.

The virial equation of state can be regarded as a systematic extension of NSE models for strong interactions in the resonant continuum. Such a comparison will also provide valuable insights how to systematically organize the virial expansion to include heavy nuclei. In addition, topics of future studies include model-independent predictions for the neutrino response of low-density nuclear matter and a detailed comparison with nuclear lattice calculations [47].

Acknowledgements

We thank S. Karataglidis for the calculation of the nucleon-alpha phase shifts and A. Marek for providing us with tables of the LS, Shen and Wolff equations of state. This work is supported in part by the US DOE under Grant No. DE-FG02-87ER40365 and the NSF under Grant No. PHY-0244822.

-
- [1] M. Liebendörfer, M. Rampp, H.-Th. Janka and A. Mezzacappa, *Astrophys. J.* **620** (2005) 840.
 - [2] R. Walder, A. Burrows, C.D. Ott, E. Livne and M. Jaraiah, *Astrophys. J.* **626** (2005) 317.
 - [3] M. Costantini, A. Ianni and F. Visanni, *Phys. Rev.* **D70** (2004) 043006.
 - [4] C. Lunardini and A.Y. Smirnov, *Astropart. Phys.* **21** (2004) 703.
 - [5] B.S. Meyer, *Ann. Rev. Astron. Astrophys.* **32** (1994) 153.
 - [6] C.J. Horowitz and A. Schwenk, *nucl-th/0507064*.
 - [7] K.M. O'Hara, S.L. Hemmer, M.E. Gehm, S.R. Granade and J.E. Thomas, *Science* **298** (2002) 2179.
 - [8] M.E. Gehm, S.L. Hemmer, S.R. Granade, K.M. O'Hara and J.E. Thomas, *Phys. Rev.* **A68** (2003) 011401(R); J. Kinast, A. Turlapov, J.E. Thomas, Q. Chen, J. Stajic and K. Levin, *Science* **307** (2005) 1296.
 - [9] T. Bourdel, J. Cubizolles, L. Khaykovich, K.M.F. Magalhaes, S. Kokkelmans, G.V. Shlyapnikov and C. Salomon, *Phys. Rev. Lett.* **91** (2003) 020402.
 - [10] M. Bartenstein, A. Altmeyer, S. Riedl, S. Jochim, C. Chin, J.H. Denschlag and R. Grimm, *Phys. Rev. Lett.* **92** (2004) 120401 and *cond-mat/0412712*.
 - [11] T.-L. Ho and E.J. Mueller, *Phys. Rev. Lett.* **92** (2004) 160404.
 - [12] T.-L. Ho and N. Zahariev, *cond-mat/0408469*.
 - [13] B. Friedman and V.R. Pandharipande, *Nucl. Phys.* **A361** (1981) 502.
 - [14] A. Akmal, V.R. Pandharipande and D.G. Ravenhall, *Phys. Rev.* **C58** (1998) 1804.
 - [15] M. Hjorth-Jensen, T.T.S. Kuo and E. Osnes, *Phys. Rept.* **261** (1995) 125; L. Engvik, G. Bao, M. Hjorth-Jensen, E. Osnes and E. Østgaard, *Astrophys. J.* **469** (1996) 794.
 - [16] M. Baldo, in *Nuclear Methods and the Nuclear Equation of State*, International Review of Nuclear Physics, Vol. 8, World Scientific, 1999.
 - [17] S.K. Bogner, T.T.S. Kuo and A. Schwenk, *Phys. Rept.* **386** (2003) 1.
 - [18] S.K. Bogner, A. Schwenk, R.J. Furnstahl and A. Nogga, *Nucl. Phys.* **A763** (2005) 59.
 - [19] J.-R. Buchler and S.A. Coon, *Astrophys. J.* **212** (1977) 807.
 - [20] S. Goriely, M. Samyn, P.-H. Heenen, J. M. Pearson and F. Tondeur, *Phys. Rev.* **C66** (2002) 024326.
 - [21] M. Bender, P.-H. Heenen and P.-G. Reinhard, *Rev. Mod. Phys.* **75** (2003) 121.
 - [22] M.V. Stoitsov, J. Dobaczewski, W. Nazarewicz, S. Pittel and D.J. Dean, *Phys. Rev.* **C68** (2003) 054312.
 - [23] P. Ring, *Prog. Part. Nucl. Phys.* **37** (1996) 193.

- [24] B.D. Serot and J.D. Walecka, *Int. J. Mod. Phys.* **E6** (1997) 515.
- [25] R.J. Furnstahl and B.D. Serot, *Nucl. Phys.* **A671** (2000) 447.
- [26] J.M. Lattimer and F.D. Swesty, *Nucl. Phys.* **A535** (2001) 331.
- [27] H. Shen, H. Toki, K. Oyamatsu and K. Sumiyoshi, *Nucl. Phys.* **A637** (1998) 435; *Prog. of Theo. Phys.* **100** (1998) 1013.
- [28] D. Lee and T. Schäfer, *Phys. Rev.* **C72** (2005) 024006.
- [29] E. Beth and G.E. Uhlenbeck, *Physica* **4** (1937) 915.
- [30] A. Pais and G.E. Uhlenbeck, *Phys. Rev.* **116** (1959) 250.
- [31] P.F. Bedaque and G. Rupak, *Phys. Rev.* **B67** (2003) 174513.
- [32] S. Ichimaru, *Rev. Mod. Phys.* **54** (1982) 1017.
- [33] S. Pratt, P. Siemens and Q.N. Usmani, *Phys. Lett.* **B189** (1987) 1.
- [34] Venugopalan and Prakash, *Nucl. Phys.* **A546** (1992) 718.
- [35] K. Huang, *Statistical Mechanics*, Wiley N.Y., Second Edition (1987). For the relation of the second virial coefficient b_2 to the two-body elastic scattering phase shifts, see p. 224-227.
- [36] V.G.J. Stoks, R.A.M. Klomp, M.C.M. Rentmeester and J.J. de Swart, *Phys. Rev.* **C48** (1993) 792; see also NN-Online, <http://nn-online.org>.
- [37] R.A. Arndt and L.D. Roper, *Phys. Rev.* **C1** (1970) 903.
- [38] K. Amos, P.J. Dortmans, H.V. von Geramb, S. Karataglidis and J. Raynal, *Adv. Nucl. Phys.* **25** (2000) 275; K. Amos and S. Karataglidis, private communication.
- [39] R.A. Arndt, D.L. Long and L.D. Roper, *Nucl. Phys.* **A209** (1973) 429.
- [40] S.A. Afzal, A.A.Z. Ahmad and S. Ali, *Rev. Mod. Phys.* **41** (1969) 247. The $\alpha\alpha$ phase shifts are taken from Table II.
- [41] A.D. Bacher, F.G. Resmini, H.E. Conzett, R. de Swiniarski, H. Meiner and J. Ernst, *Phys. Rev. Lett.* **29** (1972) 1331. The $\alpha\alpha$ phase shifts are taken from Fig. 1.
- [42] J.M. Lattimer, C.J. Pethick, D.G. Ravenhall and D.Q. Lamb, *Nucl. Phys.* **A432** (1985) 646.
- [43] J.M. Lattimer, private communication.
- [44] W. Hildebrandt, K. Nomoto and R.G. Wolff, *Astron. Astrophys.* **133** (1984) 175.
- [45] W.P. Tan, S.R. Souza, R.J. Charity, R. Donangelo, W.G. Lynch and M.B. Tsang, [nucl-th/0311001](http://arxiv.org/abs/nucl-th/0311001).
- [46] C.A. Bertulani, H.W. Hammer and U. Van Kolck, *Nucl. Phys.* **A712** (2002) 37.
- [47] C.J. Horowitz, D. Lee and A. Schwenk, in prep.